Activation of Nucleoplasmin, an Oligomeric Histone Chaperone, Challenges Its Stability[†,‡]

Stefka G. Taneva,[§] Inés G. Muñoz,[||] Guillermo Franco,[§] Jorge Falces,[§] Igor Arregi,[§] Arturo Muga,[§] Guillermo Montoya,[||] María A. Urbaneja,[*,§] and Sonia Bañuelos[*,§]

Unidad de Biofísica (CSIC−UPV/EHU) and Dpto. de Bioquímica y Biología Molecular, Universidad del País Vasco, P.O. Box 644, 48080 Bilbao, Spain, and Macromolecular Crystallography Group, Spanish National Cancer Research Centre (CNIO), c/Melchor Fdez. Almagro 3, 28029 Madrid, Spain

Received May 23, 2008; Revised Manuscript Received October 30, 2008

ABSTRACT: Nucleoplasmin (NP) is a pentameric, ring-shaped histone chaperone involved in chromatin remodeling processes such as sperm decondensation at fertilization. Monomers are formed by a core domain, responsible for oligomerization, that confers the protein a high stability and compactness and a flexible tail domain, that harbors a polyglutamic tract and the nuclear localization signal. Fully activated NP presents multiple phosphorylated residues in the tail and in flexible regions of the core domain. In this work, we analyze the effect of activation on the structure and stability of the full-length protein and the isolated core domain through phosphorylation mimicking mutations. We have solved the crystal structure of an activated NP core domain that, however, is not significantly different from that of the wild-type, inactive, NP core. Nevertheless, we find that NP activation results in a strong destabilization of the pentamer probably due to electrostatic repulsion. Moreover, characterization of the hydrodynamic properties of both full-length and core domain proteins indicates that activating mutations lead to an expansion of the NP pentamer in solution. These findings suggest that NP needs a compact and stable structure to afford the accumulation of negative charges that weakens its quaternary interactions but is required for its biological function.

Nucleoplasmin (NP)[1] is a nuclear chaperone that assists the assembly of nucleosomes during fertilization and early stages of development (*1*−*3*). In *Xenopus laevis* eggs, where it was first isolated, this highly acidic protein is thought to serve as a "storage chaperone" for core histones H2AH2B. *In vitro*, NP is able to decondense the highly packed sperm chromatin, displacing its specific basic proteins, and it has been proposed that, upon fertilization, it replaces sperm-specific proteins by histones H2AH2B (*1, 2*). Besides its active role in fertilization, NP is also involved in other chromatin remodeling processes, namely replication licensing (*4*) and pluripotent cell reprogramming (*5*).

NP is a homopentamer, composed of 200 residue subunits, each built of two domains named core and tail. The core domain corresponds to the N-terminal 120 residues and is responsible for protein oligomerization. Three-dimensional structures of the recombinant *Xenopus* NP core domain (ref *6*; see Figure 1) and the core domains from the homologous proteins dNLP from *Drosophila* (*7*) and NO38 from *Xenopus* (*8*) have been solved. The structures consist of an eight-stranded β-barrel with a jelly roll topology, forming a ring of 60 Å diameter and 40 Å height (Figure 1). This core domain confers an extreme stability to NP (*9*), mainly due to a conserved network of hydrophobic interactions between the pentamer subunits (*6*). The C-terminal tail domain contains a segment rich in negatively charged amino acids (termed "polyglu" or A2) and a nuclear localization signal. It adopts a flexible or nonregular conformation (*9, 10*), also known as "natively disordered" (*11*).

NP is activated by phosphorylation of multiple serine/threonine residues, along both core and tail domains (*10, 12, 13*). The level of phosphorylation gradually increases during egg maturation, reaching an average of 7−10 phosphates per monomer, so that at the time of fertilization the activity of the protein is maximum. One approach to understand the activation mechanism of NP is to analyze the impact of phosphorylation of specific residues on the protein activity and conformation. Recently, we have identified by mass spectrometry most of the phosphoresidues of

[†] This work was supported by the Ministerio de Educación y Ciencia (Grant BFU2007-64452), Basque Government (IT-358-07), and Diputación Foral de Vizcaya (Grant DIPE06/20). G.M. acknowledges funding support from the Ministerio de Educación y Ciencia (Grant BFU2005-02403). S.G.T. is a visiting professor at the University of the Basque Country and associate member of the Institute of Biophysics, Bulgarian Academy of Sciences. J.F. and I.A. hold predoctoral fellowships from the University of Basque Country and from the Ministerio de Educación y Ciencia, respectively, and S.B. is supported by a Ramón y Cajal contract.

[‡] The structure presented within this study has been deposited in the Protein Data Bank, its ID code being 2vtx.

* Corresponding authors. E-mail: mariaangeles.urbaneja@ehu.es; sonia.banuelos@ehu.es. Telephone: +34 94 601 3352. Fax: +34 94 601 3360.

[§] Universidad del País Vasco.

[||] Spanish National Cancer Research Centre.

[1] Abbreviations: NP, nucleoplasmin; wtNP, wild-type full-length NP; wtCORE, wild-type core domain; DSC, differential scanning calorimetry; CD, circular dichroism; DLS, dynamic light scattering; GuSCN, guanidinium thiocyanate; E_a, activation energy; C_p, absolute heat capacity; D_{50}, denaturant concentration at the transition midpoint; T_m, unfolding transition temperature.

10.1021/bi800975r CCC: $40.75
Published on Web 12/04/2008

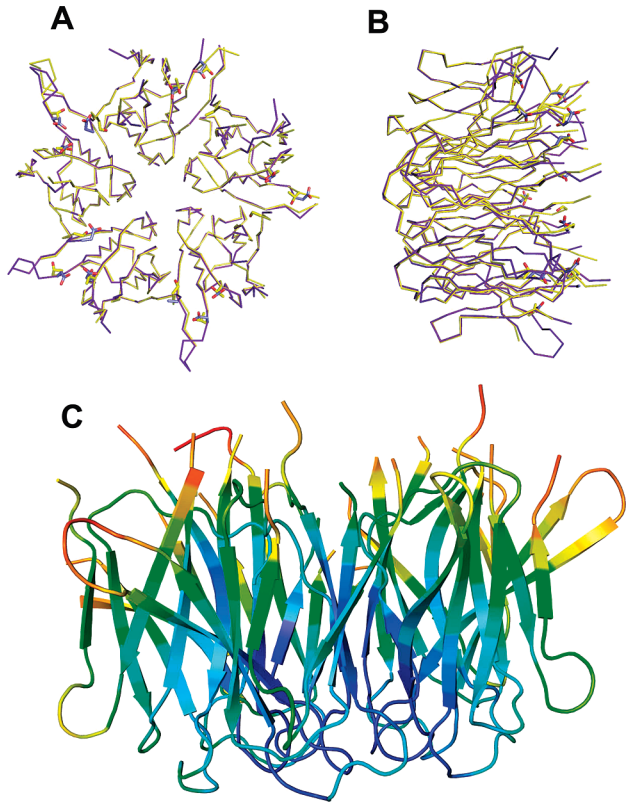

FIGURE 1: Crystal structure of CORE8D. Cα trace superposition of the 3D structures of the wild-type NP core domain (6) (yellow) and CORE8D mutant (purple). (A) Top view from the distal face. (B) Side view. The side chains of the wild-type and mutated residues (at positions 15, 66, and 96) are displayed as sticks showing the differences in orientations between the wild-type and the mutant structure. (C) Representation of the CORE8D structure colored by *B* factors. Red corresponds to relatively high *B* factors; blue corresponds to low *B* factors. The pentamer is oriented with the distal face up.

natural, egg NP (*13*). Given that natural NP is heterogeneously phosphorylated and that it is not feasible to phosphorylate the protein *in vitro* with significant yield, we have used in previous studies the strategy of mutating those and other phosphorylatable residues for aspartic acid to mimic the presence of phosphoryl groups (*13, 14*). In contrast to nonphosphorylated recombinant NP, we have proven that these mutants are active in sperm chromatin decondensation (*13, 14*). Selective mutation within the core and/or tail domains of NP has allowed us to analyze the contribution of each domain to the activation mechanism and conclude that phosphorylation of both protein domains is necessary to achieve full activation (*13*).

Chemical denaturation of this pentameric protein has been recently characterized (*15*): NP unfolds in a two-state process, in which the pentamer dissociates and concomitantly denatures ($N_5 \leftrightarrow 5$ U). Natural, active NP is less stable than the nonphosphorylated protein (*10, 15*). In the present study, by taking advantage of the phosphorylation-mimicking mutations, we attempt to analyze the effect of activating modifications in the structure and stability of NP domains. We find that although the crystal structure of an active NP core domain mutant can be superimposed onto the wild-type NP (*6*), the stability of the activated mutants steadily decreases, and their structures suffer an expansion in solution. The comparison of the different mutant's stability by differential scanning calorimetry (DSC) and chemical unfolding experiments points to an activation-induced destabilization of NP. These results agree with a previous study on natural NP variants (*15*) and suggest an explanation for the extreme stability of this protein.

Table 1: Data Collection and Refinement Statistics

Data Collection[a]	
environment	ADSC detector, ESRF, beamline ID14ih4
wavelength	0.9198 Å
space group	$P2_12_12_1$
cell dimensions (Å; deg)	$a = 67.03$, $b = 94.6$, $c = 176.1$; $\alpha = \beta = \gamma = 90$
no. of molecules in asymmetric unit	2
resolution (Å)	40.0−2.5 (2.64−2.50)
unique reflections	57758
redundancy	6.0 (6.1)
data cutoff	$F > 0$
completeness	100 (100)
R_{merge}[b]	0.07 (0.31)
$\langle I/\sigma(I)\rangle$	7.7 (17.5)
Refinement	
no. of reflections (completeness, %)	37569 (99.98)
resolution range (Å)	40.0−2.50
R-factor/*R*-free (%)	18.23/26.90
no. of protein atoms (average *B*, Å^2)[c]	7086 (48.60)
no. of water molecules (average *B*, Å^2)[c]	175 (45.46)
rmsd bond length (Å)	0.034
rmsd bond angle (deg)	2.483
Ramachandran plot outliers (%)[d]	5 (0.7)

[a] Values in the highest resolution shell are given in parentheses. [b] $R_{merge} = \sum_\eta\sum_\tau|I_{\eta,\tau} - \langle I_\eta\rangle|/\sum_\eta\sum_\tau|I_{\eta,\tau}|$. [c] Calculated using MOLEMAN. [d] Calculated using PROCHECK.

EXPERIMENTAL PROCEDURES

Protein Expression and Purification. NP constructs were cloned in pET11b (*10, 13, 14*), induced with 1 mM IPTG, and overexpressed for 15−20 h at 18 °C in *Escherichia coli* BL21 (DE3) cells. Proteins were purified as described previously for full-length constructs (*13*), wtCORE (*9*), and mutated core domains (*14*). In the final purification step, all constructs were loaded onto a Superdex 200 16/60 column equilibrated with 25 mM Tris-HCl, pH 7.5, and 100 mM NaCl. After checking that they were free of contaminating DNA by UV absorbance spectroscopy, they were concentrated up to 20−40 mg/mL and frozen in liquid N_2 for storage. Protein concentration was determined by the BCA colorimetric assay (Pierce) and occasionally by amino acid analysis. We have observed a small proportion of degradation products in NP mutants, being at most 11% as estimated by densitometry of SDS−PAGE gels (not shown).

X-ray Crystallography. Mass spectrometry confirmed that CORE8D was comprised by 119 out of the 120 expected residues. Only the first methionine is missing, a fact that quite often occurs during protein expression in bacteria when the second residue is small and uncharged (*16*). Crystals were grown in hanging drops including 15 mg/mL protein, 100 mM sodium acetate, pH 4.6, 20 mM $CaCl_2$, and 30% (v/v) 2-methyl-2,4-pentanediol (MPD). A complete X-ray diffraction data set was collected at 100 K from a single crystal using synchrotron radiation. Statistics for the crystallographic data are summarized in Table 1. Approximately 5% of the reflections were set aside for free *R*-factor calculations during refinement (*17*). The structure was solved using the molecular

replacement method as implemented in the program EPMR (*18*). The search model was the *X. laevis* NP core found in the Protein Data Bank (*6*) (entry 1K5J), using the program CLUSTALW (*19*). Refinement was carried out with REFMAC5 (*20*) and included rigid-body refinement. A $2F_o - F_c$ map showed clear and contiguous electron density for most of the peptide backbone and side chains of the protein. Several rounds of rebuilding using the program O (*21*) and the placement of water into the electron density resulted in the structure described here. The electron density map was subjected to density modification including solvent flattening (~42% solvent) and NCS 5-fold averaging in DM (*22*). The geometry of the model was checked with PROCHECK (*23*), and the majority of residues were found in allowed regions of the Ramachandran map. Coordinates for the final model, and the corresponding structure factor data, have been deposited in the PDB with entry code 2vtx.

Differential Scanning Calorimetry (DSC). DSC scans were performed in a VP-DSC microcalorimeter (Microcal, Northampton, MA). Prior to measurements, samples were dialyzed against 10 mM phosphate buffer and 1 mM EGTA, pH 7.0, except for the analysis of stability as a function of pH, when pH was varied between 2.0 and 7.0. For the pH range between 2.0 and 4.0, 25 mM Gly-HCl was also used. Samples were properly degassed and run under an extra pressure of around 28 psi. It should be noted that at this pressure, that prevents sample boiling, T_m values above 100 °C can be measured. Protein concentration was generally 0.3−0.7 mg/mL and scan rate 60 °C/h, except for the absolute heat capacity (C_p) calculation, where the concentration was varied between 0.1 and 1.5 mg/mL, and activation energy (E_a) calculation, where scan rates between 10 and 90 °C/h were used. The absolute heat capacity C_p was calculated according to Kholodenko and Freire (*24*): the excess heat capacity c_p at 37 °C was plotted versus the protein mass in the calorimetric cell, and the absolute C_p was obtained from the expression:

$$m = C_p - v_p$$

where m is the slope of the linear regression of this plot and v_p is the partial specific volume of the protein (0.73 cm^3/g in the case of NP (*25*)). r^2 of the regression was 0.999 for wtCORE and 0.945 for CORE8D.

The activation energy, E_a, was obtained from (i) the values of the rate constant of the transition, k, at a given temperature (*26, 27*):

$$k = A \exp(-E_a/RT) \quad (1)$$

where E_a is the activation energy and A is the frequency factor.

The rate constant of the reaction at a given temperature T is given by

$$k = \nu c_p/(Q_t - Q) \quad (2)$$

where ν is the scanning rate (K/min), c_p is the excess heat capacity at a given temperature, Q is the heat evolved at that temperature, and Q_t is the total heat of the calorimetric transition.

The E_a was obtained from (ii) the dependence of the heat capacity evolved with temperature expressed as

$$\ln[\ln Q_t/(Q_t - Q)] = E_a/R(1/T_m - 1/T) \quad (3)$$

The E_a was obtained from (iii) the heat capacity c_p^m at the transition temperature T_m, where the activation energy can also be calculated by the equation:

$$E_a = eRT_m^2 c_p^m/Q_t \quad (4)$$

Chemical Unfolding Experiments. NP unfolding reactions were performed in 50 mM phosphate buffer, pH 6.5, containing varying concentrations of denaturants (0−10 M for urea and 0−3 M for GuSCN), using a protein concentration between 0.1 and 1.1 mg/mL, after incubation for 3 h with GuSCN and 12 h with urea at 25 °C. Native and denaturant-treated NP samples were excited at 280, and their fluorescence emission spectra were recorded between 290 and 450 nm in a SLM-8100 spectrofluorometer (Aminco) at 25 °C, using 0.3 × 0.3 cm cuvettes and slits width of 4 nm. Spectra were corrected for solvent signal and inner filter effect. NP unfolding was monitored following the λ_{em} shift, the fluorescence intensity at λ_{em}, and the steady-state Trp anisotropy. Reversibility of the chemical unfolding process was checked by denaturing the proteins, dialyzing them in native buffer for refolding, and analyzing their fluorescence emission properties. The denaturation process was fitted to a two-state transition with the native pentamer converting directly to denatured monomers ($N_5 \leftrightarrow 5U$).

ANS Binding. The change in hydrophobic surface access of the proteins was studied upon addition of 15 μM 1,8-ANS to 100 μL of protein sample (1.3 mg/mL). Fluorescence spectra of the samples were recorded with λ_{ex} set at 375 nm. The excitation and emission slits were 4 nm.

Circular Dichroism (CD) Spectroscopy. CD spectra were measured at 25 °C on a Jasco 720 spectropolarimeter, using cuvettes with a path length of 0.02 cm and protein concentration of 0.5 mg/mL in 10 mM Tris-HCl and 50 mM NaCl, pH 7.4. Mean residue ellipticity values were calculated using the expression $\Theta = \epsilon/10cln$, where ϵ is the ellipticity (millidegrees), c the protein concentration (mol/L), l is the path length (cm), and n is the number of peptide bonds (199 for NP). Estimation of the secondary structure content was done with the program CDSSTR of the server DICHROWEB (*28*) (http://www.cryst.bbk.ac.uk/cdweb), using as reference the SP175 database (*29*).

Gel Filtration Chromatography. Chromatography was performed in a Superdex 200 HR (General Electrics) column equilibrated with 25 mM Tris-HCl and 100 mM NaCl, pH 7.5, at room temperature and a flow rate of 0.4 mL/min, and injecting the protein at a concentration of 10−12 mg/mL.

Dynamic Light Scattering (DLS). DLS measurements were made with a Nano-S Zetaseizer (Malvern Instruments, U.K.), using a red laser (633 nm), at room temperature, in 25 mM Tris-HCl and 100 mM NaCl buffer, pH 7.5. Protein concentration was 2.5 mg/mL.

RESULTS

Crystal Structure of an Active NP Core Domain. We previously found that the phosphorylated core domain isolated from egg nucleoplasmin, as well as an activated recombinant core in which eight phosphorylatable residues were replaced by Asp, is able to dissociate linker-type histones from DNA and decondense sperm chromatin (*14*). For a better understanding of the conformational consequences of phosphorylation-mimicking mutations that lead

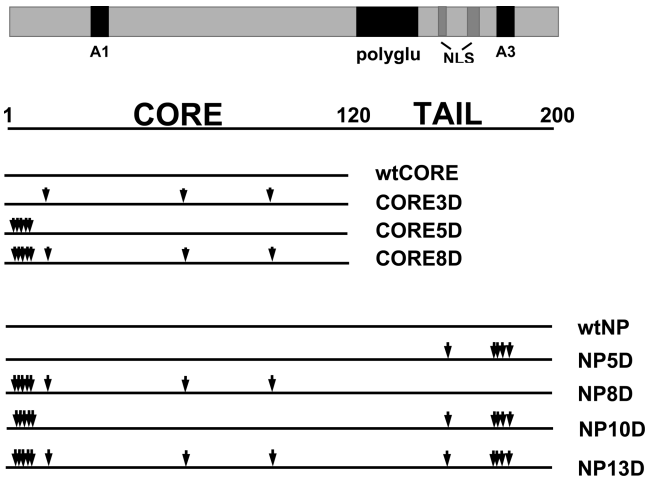

FIGURE 2: NP mutants used in this study. Scheme representing NP domains and the positions of the substitutions of phosphorylatable residues for Asp (arrowheads), in both the full-length and core domain constructs. The three acidic tracts (A1, A2 or "polyglu", and A3) (*1*), as well as the nuclear localization signal (NLS) are depicted.

to activation of the NP core domain, we have solved by X-ray crystallography the 3D structure of mutant CORE8D (corresponding to NP residues 1−120, with amino acids 2, 3, 5, 7, 8, 15, 66, and 96 substituted for Asp; see below) at 2.5 Å resolution (Table 1 and Figure 1). Surprisingly, the structure of this protein, the first one of an active form of NP, is very similar to that of the wild-type NP core domain (*6*), with rmsd between 451 Cα atoms of the pentamer being 0.65 Å (Figure 1A,B). In our structure, the loop between strands β2 and β3, containing the acidic tract A1, that has been implicated in histone binding (*30*) is better defined than in the published wtCORE structure (*6*), and only three residues (35−37) are still not visible. Figure 1C represents the CORE8D structure colored by *B* factors. The fact that the distal face of the pentamer is characterized by comparatively higher *B* factors reflects a higher flexibility of this region and might support the notion that it is involved in the interaction with NP ligands (*2*). Given that the X-ray structures of both proteins are so similar, we next sought to analyze the following conformational properties of the proteins in solution: secondary structure, stability against temperature and chemical reagents, and hydrodynamic properties.

Effect of Activating Mutations in NP Core Domain. Although the crystal structures of wtCORE and CORE8D are practically identical, their dynamic behavior in solution might differ. In order to explore this possibility, several properties of four core domains, in which different phosphorylated (*13*) and phosphorylatable residues were replaced by Asp, were analyzed. We mutated residues 2, 3, 5, 7, and 8, generating the mutant CORE5D, residues 15, 66, and 96, generating CORE3D, and a combination of both in CORE8D (Figure 2). Note that our sequence numbering starts after the N-terminal Met, since we found it to be absent in natural NP (*13*) and in recombinant CORE8D (see Experimental Procedures). As stated above, the activity of CORE8D, measured as the ability to decondense *Xenopus* sperm and to extract sperm basic proteins and linker histones from chromatin, is similar to that of the core domain obtained by proteolysis of hyperphosphorylated egg NP (*14*). In natural,

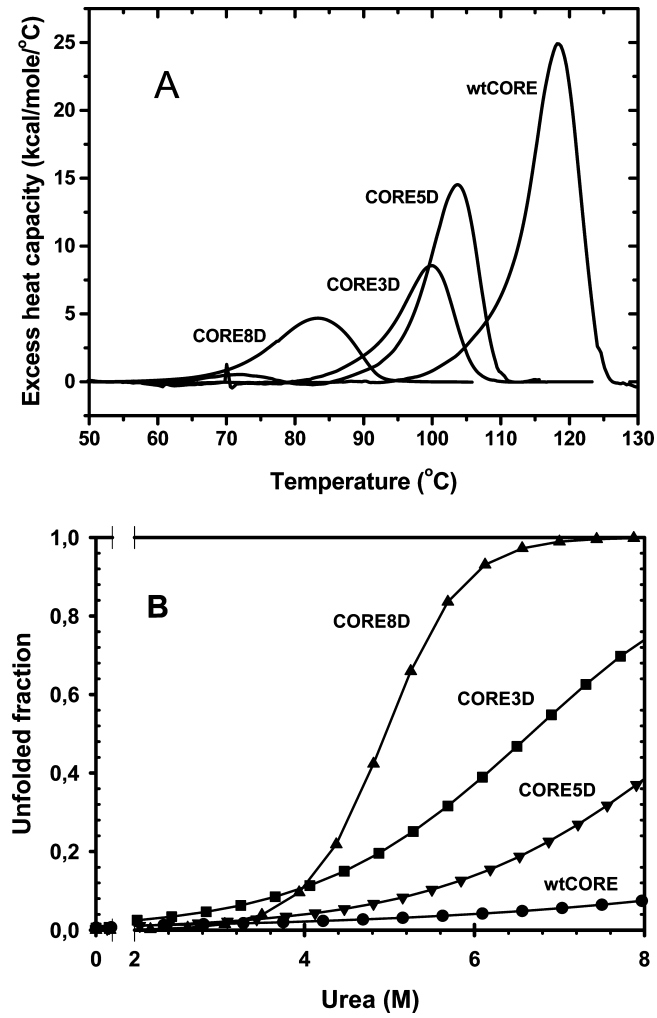

FIGURE 3: Effect of phosphorylation-mimicking mutations on NP core domain thermal and chemical stability. (A) DSC thermograms of wtCORE, CORE3D, CORE5D, and CORE8D, in 10 mM phosphate buffer and 1 mM EGTA, pH 7.0. (B) Urea-induced unfolding of the same NP variants, followed by intrinsic fluorescence anisotropy in 50 mM phosphate buffer, pH 6.5, at 25 °C and fitted to a two-state process.

hyperactivated protein (*Xenopus* egg NP), there are at least four phosphoryl groups in the first 15 N-terminal residues (*13*). Among the mutated residues, only 15, 66, and 96 are seen in the crystal structure of NP core domain and lie on the same face (termed "distal") of the NP pentamer. Although no experimental evidence exists so far for phosphorylation of residues 66 and 96, the facts that CORE5D is less active than CORE8D (*14*) and that a full-length mutant lacking substitutions at 15, 66, and 96 (NP10D) is only partly active (see below) suggest that mutations at the distal surface in the folded core domain might be required to mimic the function of the egg NP core.

Comparison of the thermal unfolding profiles of NP core domains indicates that the activating mutations strongly decrease NP thermal stability (Figure 3A and Table 2). The mutant with three substitutions is less stable than CORE5D (mutated in five positions), being CORE8D, as expected, the least stable. The mutant's stability toward chemical denaturation has also been analyzed. As previously found for full-length NP (*15*), chemical unfolding of the isolated core domain is reversible and follows a two-state mechanism ($N_5 \leftrightarrow 5U$), according to which pentamer dissociation simulta-

Table 2: Thermodynamic Parameters of NP Thermal and Chemical Denaturation[a]

protein	T_m (°C)[b]	ΔH_{cal} (kcal/mol)[b]	E_a (kcal/mol)[b]	D_{50}[urea] (M)[b]
wtCORE	117.6	244.7	69.8	nd[c]
CORE3D	100.1	88.9		6.89[d]
CORE5D	103.6	138.1		nd[c]
CORE8D	83.1	68.4	52.1	4.92
wtNP	110.1	157.2		8.35[d]
NP5D	100.2	93.2		7.69[d]
NP8D	76.3	57.3		2.88
NP10D	88.0	91.4		5.39
NP13D	55.2	17.9		2.63
egg NP	75.0	50.0		3.52

[a] Unfolding transition temperatures, T_m, calorimetric denaturation enthalpies, ΔH_{cal}, and denaturant concentrations at transition midpoints, D_{50}, are shown for the different core domain and full-length NP mutants. DSC scans were run in 10 mM phosphate buffer and 1 mM EGTA, pH 7.0. Chemical unfolding experiments were performed in 50 mM phosphate buffer, pH 6.5 at 25 °C. Activation energies, E_a, were calculated for wtCORE and CORE8D. ΔH_{cal} and E_a are given per mole of monomer. For comparison, T_m and ΔH_{cal} (*39*) as well as D_{50} (*15*) of egg NP are included. [b] The maximum standard deviation between experiments was 1.5 °C for T_m, 36 kcal/mol for ΔH_{cal}, 0.08 M for D_{50}, and 2.6 kcal/mol for E_a. [c] In the case of wtCORE and CORE5D, which at 8 M urea are still (partially) folded, D_{50} cannot be determined (nd). [d] To estimate D_{50} of CORE3D, wtNP, and NP5D, we assume that if urea fully unfolded these mutants, the emission wavelength of its denatured state would be the same as those of CORE8D and NP13D, respectively.

neously occurs with protein unfolding, rendering five unfolded monomers (data not shown). The same destabilization pattern of the different mutants observed by DSC is also confirmed with urea-induced chemical denaturation (Figure 3B). Albeit this denaturant completely unfolds neither wtCORE nor CORE5D, the comparison confirms that CORE3D, in spite of carrying fewer substitutions, is less stable than CORE5D. Mutation-induced destabilization could be due to enhanced electrostatic repulsion in the oligomer, which at neutral pH is already negatively charged. The higher sensitivity of the protein stability to mutations in residues 15, 66, and 96 might be due to the fact that these residues are located in a "structured" region, whereas the other replacements, that apparently do not have such impact on stability, affect residues in a flexible protein segment, which could be reallocated by the protein to compensate their destabilizing effect.

Thermal unfolding of the core domain is an irreversible process (data not shown). We have employed a simplified "two-state irreversible" kinetic model (*26, 31*) to analyze the thermal denaturation of wtCORE and CORE8D at different heating rates. According to this model an irreversible protein denaturation can be described by a scanning rate-dependent transition between two states, native and irreversibly denatured. Different mathematical expressions, using diverse experimental information from the calorimetric transition, were developed to calculate the activation energy (E_a) of the denaturation transition (*26, 27*). Analysis of the DSC curves obtained at different scan rates (see Experimental Procedures; data not shown) gives E_a values of 69.8 ± 2.6 and 52.1 ± 2.4 kcal/mol for wtCORE and CORE8D, respectively. Therefore, the activation energy of thermal-induced unfolding is higher for wtCORE than for CORE8D. Since the kinetic stability of a protein is a result of the energy barrier between the folded and unfolded states, our data suggest that wtCORE is kinetically more stable than CORE8D. Thus phosphorylation-mimicking mutations reduce the energy barrier of the transition from the folded to unfolded state in the NP core domain.

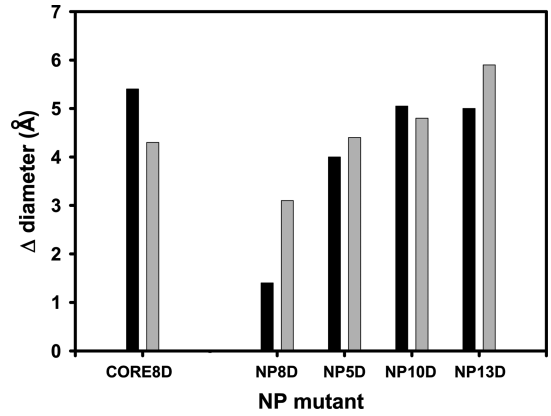

FIGURE 4: Mutation-induced expansion of NP. Bar graph representing the increase in particle diameter (double of Stokes radii estimated from gel filtration chromatography (black bars) and measured by DLS (gray bars)) of the different NP mutants as compared to the wild-type recombinant core domain (77.2 and 64.5 Å by chromatography and DLS, respectively) and the full-length recombinant protein (97.2 and 93.7 Å by chromatography and DLS, respectively). Polydispersity (PdI) values for the different samples varied between 0.045 and 0.200. Both chromatography runs and DLS measurements were performed in 25 mM Tris-HCl and 100 mM NaCl buffer, pH 7.5.

The strong destabilization effect of the activating substitutions suggests a mutation-induced conformational change. But the fact that the mutants are active and display a cooperative unfolding transition (see Figure 3A) indicates that they are folded. Furthermore, far-UV CD demonstrates that none of the mutants show significant alterations of the wtCORE secondary structure (not shown), in agreement with X-ray data. To further characterize the conformational change associated with protein activation, the excess heat capacity c_p of wtCORE and CORE8D was measured at various protein concentrations to calculate the absolute heat capacity, C_p, of their native state (at 37 °C) (*24*), which is related to solvent exposure of protein hydrophobic groups (*32*). The C_p values, 0.23 and 0.42 cal K^{-1} g^{-1} for wtCORE and CORE8D, respectively, suggest faster dynamics or higher conformational fluctuations in CORE8D (*33*). We have also compared the hydrodynamic properties of wtCORE and CORE8D by size exclusion chromatography. The mutant clearly behaves as a bigger particle than wtCORE (estimated MW 99935 and 75573 Da, respectively), suggesting that phosphorylation-mimicking mutations induce an expansion of the protein particle (Figure 4). Dynamic light scattering measurements (Figure 4) further corroborate the larger dimensions of CORE8D (average diameter 68.8 Å), as compared with wtCORE (64.5 Å). Taken together, these results suggest that the activating mutations induce a destabilization of the core particle that as compared with the inactive wild-type recombinant core shows (i) an increase in size and (ii) faster dynamics without affecting the overall protein structure.

Effect of Activating Mutations in Full-Length NP. Before introducing this section, it is worth to analyze the contribution of each domain to the stability of wild-type full-length NP. Chemical unfolding of NP with guanidinium thiocyanate (Figure 5A), as previously described, results in a cooperative transition with D_{50} = 1.78 M denaturant that can be

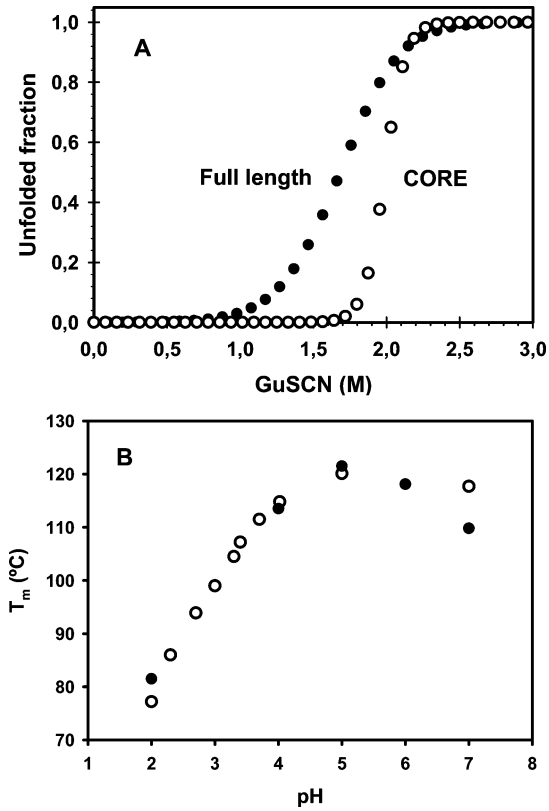

FIGURE 5: Comparison of full-length NP and core domain stability. (A) GuSCN-induced unfolding of full-length NP (●) and core domain (○) followed by the change in intrinsic fluorescence and fitted to a two-state process. Experiments were done in 50 mM phosphate buffer, pH 6.5, at 25 °C. (B) Plot of T_m of full-length NP (●) and core domain (○) as a function of pH. Thermal scans were made in 25 mM Gly-HCl and 1 mM EGTA buffer (between pH 2.0 and pH 4.0) and 10 mM phosphate buffer and 1 mM EGTA (between pH 4.0 and pH 7.0).

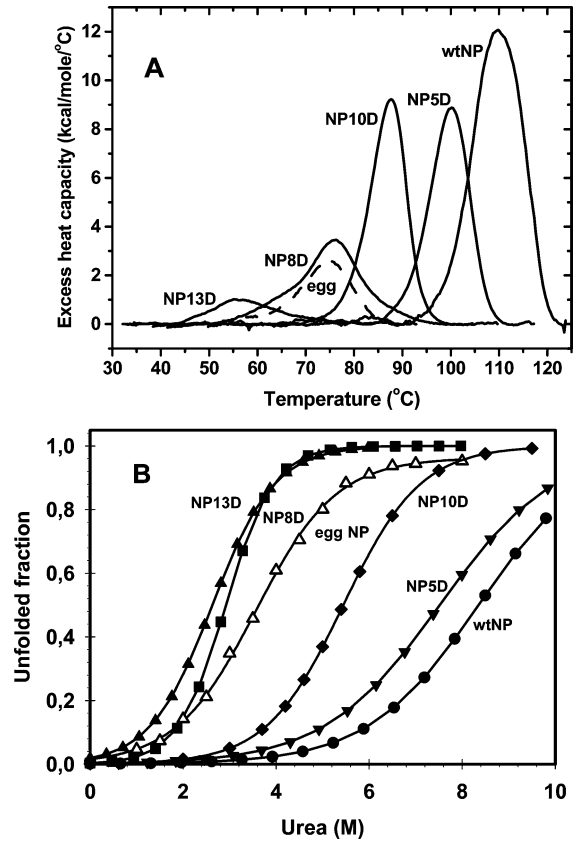

FIGURE 6: Effect of phosphorylation-mimicking mutations on full-length NP stability. (A) DSC thermograms of wtNP, NP5D, NP8D, NP10D, and NP13D, in 10 mM phosphate buffer and 1 mM EGTA, pH 7.0. For comparison, a scan of egg NP (*39*) has been included. (B) Urea-induced unfolding of the same NP variants, followed by intrinsic fluorescence spectroscopy, measured in 50 mM phosphate buffer, pH 6.5, at 25 °C. The plot of egg NP has been taken from ref *15*.

adequately fit to a two-state reaction ($N_5 \leftrightarrow 5U$), with a $\Delta G_{H_2O,25°C}$ of −48 kcal/mol of pentamer (*15*). The corresponding values for the NP core domain (residues 1−120), 1.99 M and −62 kcal mol^{-1}, indicate that the stability of this protein is solely due to the core domain, while the flexible and negatively charged tails have a destabilizing contribution to the overall protein stability. The unfolding transition of the core domain is more cooperative than that of the full-length protein, as expected considering the compact structure of the core and the flexible nature of the tail domain (*10*).

Our previous analysis of NP thermal unfolding (*9*) at neutral pH had also established that the NP core domain is more stable than the full-length protein. In this work, we have compared the thermal stability of both proteins as a function of pH, finding that both reach their highest value at pH 5.0, i.e., close to their p*I* (4.81 and 5.03 for the full-length protein and the core domain, respectively, calculated on the basis of their amino acid sequence) (Figure 5B). At this pH, T_m values of full-length NP and the core domain are almost equivalent (∼120 °C), indicating that charge neutralization diminishes the unfavorable electrostatic contributions of the tail domain to the pentamer thermal stability. Below pH 4.0, the stability of both the full-length NP and core domain drops steadily, as is commonly observed for other proteins (*34*).

To understand the contribution of both NP domains to its activation mechanism, we introduced various mutations in the full-length protein. We generated a mutant named NP8D carrying eight substitutions in the core domain (the same as CORE8D) and none in the tail. As mass spectrometry analysis of egg NP identified at least four phospho residues in the tail domain (*13*), we created another mutant, NP5D, with replacement of Ser and Thr residues by Asp only within the tail domain, in positions 159, 176, 177, 181, and 183. The mutant designated NP10D presents the mutations on the flexible N-terminal region, corresponding to CORE5D, plus the above-mentioned five substitutions within the tail domain. Finally, the mutant NP13D combines the substitutions of NP8D and NP5D. Functional characterization of mutants NP5D, NP8D, and NP13D was described elsewhere (*13*) and revealed that the mutations in the core domain conferred the protein (NP8D) higher activity than those in the tail domain (NP5D) (*13*). We have recently analyzed the activity of the NP10D finding that it is similar to NP8D (data not shown). Although all mutants are able to decondense chromatin, NP13D, that harbors substitutions throughout the whole protein, is the most active and displays functional properties similar to those of natural hyperactivated egg NP (*13*). As was observed for the core domain, activating mutations cause destabilization of full-length NP toward both thermal and chemical denaturation (Figure 6 and Table 2). Substitutions located at the core domain affect the protein stability to a

greater extent: ΔT_m, as compared with wild-type NP, is approximately 34 and 10 °C for NP8D and NP5D, respectively, and the difference in D_{50} value for the dissociation and unfolding of the protein is 5.47 and 0.66 M urea, respectively, as compared to wtNP. This difference cannot be explained solely by the different number of negative charges, but reflects, as discussed previously for the core domain, that addition of charges on structurally well-defined positions (in the core domain) is more deleterious for the protein stability than at the flexible tail domain, which can also be inferred from the comparison of the stabilities of NP8D and NP10D.

NP13D, the most active mutant (displaying an activity level similar to that of egg NP), is also the most unstable (Figure 6). It presents a D_{50} value 5.72 units lower than wtNP, and analysis of its chemical unfolding curve yields a $\Delta G_{H_2O,25°C}$ of −33 kcal/mol, that corresponds to a loss of thermodynamical stability of 12 kcal/mol as compared to wtNP, and is in good agreement with data published for egg NP (*15*). Given that the denaturation process of NP accommodates to dissociation of the pentamer particle and concomitant unfolding of the resulting monomers, lower values in D_{50} reflect a higher propensity to dissociate and unfold in the presence of denaturant, suggesting that NP quaternary structure is weakened and/or more fluctuating. We compared the accessible hydrophobic regions in wtNP and NP13D using the hydrophobic fluorescent probe 1,8-ANS (1-naphthalene-8-sulfonic acid). The quantum yield of this probe, very low in polar environment, increases upon binding to hydrophobic surfaces. Upon treating wtNP and the phosphorylation-mimicking mutant NP13D with ANS, the fluorescence intensity of the probe is relatively higher when bound to the mutant (data not shown). This result suggests that the presence of activating mutations favors the existence of more accessible hydrophobic regions in NP.

The thermal stability drop of NP13D ($\Delta T_m \sim 55$ °C taking wtNP as reference) is higher than the sum of the destabilizing effects produced by the core and tail groups of mutations, rendering this active mutant less stable than egg NP. Not unexpectedly, the functional and stability properties of NP13D are similar but not identical to egg NP. Experimental evidence had indicated that egg NP is heterogeneously phosphorylated at an average of 7−10 residues per monomer (*10*), and at least seven phosphorylated residues were identified (*13*). Taking into account that at neutral pH aspartic acid has one negative charge while a phosphoryl group would display an average net charge of −1.5 (*35*), the presence of 13 Asp residues results in a reasonable approximation of the average of 7−10 phosphates, but it should be noted that the exact electrostatic and conformational properties of the native and mutated pentamer should not necessarily be the same. The mutation-induced destabilization of NP is further reflected by the tendency of the mutants to suffer proteolytic degradation during purification from the heterologous system *E. coli* (*13*). Interestingly, the thermodynamic parameters (T_m, ΔH_{cal}) of egg NP are similar to those of NP8D (Figure 6).

As seen above for the core domain, the electrostatic repulsion caused by the phosphorylation-mimicking mutations appears to induce an expansion of the full-length protein. To characterize the compactness of the different protein variants, they were compared by size exclusion chromatography (Figure 7A). Activating mutations induce

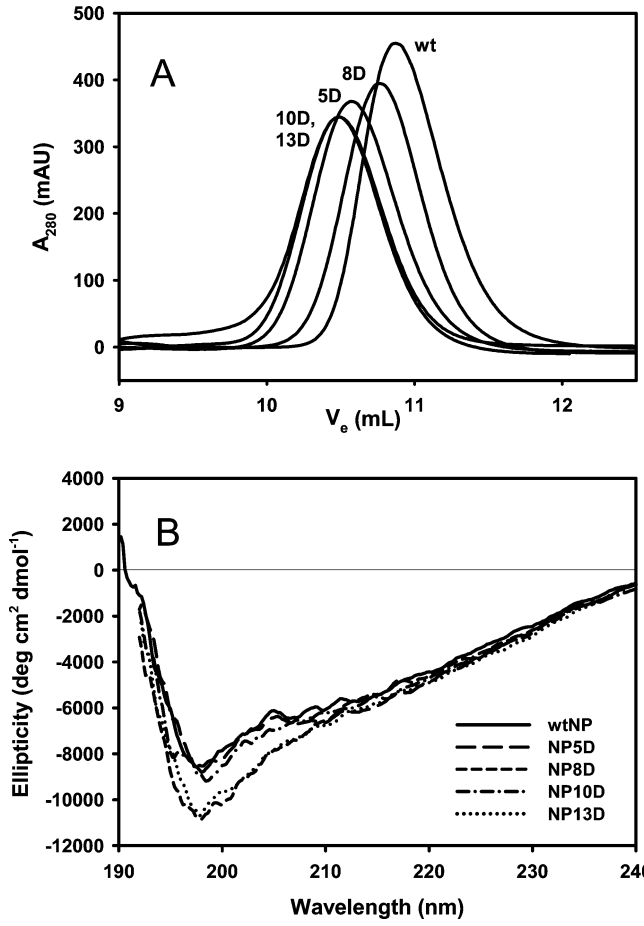

FIGURE 7: Effect of phosphorylation-mimicking mutations on NP conformational properties in solution. (A) Elution profiles of wild-type NP and mutants run on a Superdex 200 HR column, in 25 mM Tris-HCl and 100 mM NaCl, pH 7.5, at room temperature. Sizes estimated from their elution volumes are given in Figure 4. (B) Far-UV CD spectra of the same NP variants. Measurements were done in 10 mM Tris-HCl and 50 mM NaCl buffer, pH 7.4, at 25 °C.

a steady decrease in the elution volume of full-length NP, in good agreement with the described behavior of natural NP (e.g., V_e egg NP < oocyte NP < recombinant NP) (*10*), reflecting an opening and/or expansion of the NP particle upon activation. We also analyzed the effect of mutations in the core, tail, or both domains by DLS, observing that the mutants carrying substitutions in the tail domain (NP5D, NP10D, and NP13D) showed a larger apparent size as compared to wtNP and NP8D (Figure 4), which suggests that phosphorylation-mimicking mutations induce a conformational rearrangement that particularly affects the tail domain.

To explore the possible influence of activating mutations in the structure of full-length NP, we have compared the different mutants by far-UV CD spectroscopy (Figure 7B). The spectra display negative peaks at 198 nm, which arises from nonregular conformations, and 213 nm, coming mainly from the contribution of the core β structure (*9*). Parallel to what has been described for natural NP variants (*10*), the phosphorylation-mimicking mutations do not seem to imply significant effects on NP secondary structure, as judged by the similar shape of the CD spectra of the different mutants. Moreover, estimation of the secondary structure composition from the CD spectra gives percentages of α-helix (4%),

β-strand (38%), and turns plus unordered structure (57%) that differ in only 1% among the different mutants. The near-UV CD spectrum of NP is featureless and does not allow to analyze changes in the tertiary structure of the protein. Furthermore, a comparison by FTIR spectroscopy of wtNP and NP13D reveals that their secondary structure is similar (data not shown), once more paralleling the conformational features of egg NP (*10*). Taken together, these data indicate that NP activation does not involve significant changes in the secondary structure of the full-length protein but seems to affect the quaternary structure by inducing a destabilization and expansion of the pentameric particle due to electrostatic repulsion.

DISCUSSION

Nucleoplasmin-induced chromatin remodeling involves extraction of sperm-specific basic proteins or linker chromatin-associated histones (*36*) and requires phosphorylation of multiple protein residues. While phosphorylation is an ubiquitous cellular mechanism that regulates protein function (*37, 38*), NP extensive modification (average of 7−10 phosphoryl groups per protein subunit) is uncommon and results in the amplification of the acidic nature of the protein. Our results show that phosphorylation-induced activation of NP involves (i) a strong destabilization of the pentameric protein particle with subtle changes of its secondary structure and (ii) a progressive expansion of the protein oligomer that parallels its activation degree. Interestingly, these observations cannot be explained by the 3D structure of the mutated NP core domain (CORE8D) that, in contrast to wtCORE, is active in sperm decondensation and therefore able to extract linker-type histones from chromatin (*14*). The comparison of the 3D structure of both core domains reveals that they are very similar, and thus the strong activation-associated protein destabilization does not involve significant structural changes as far as the crystal structure of the core domain is concerned. However, the awareness of phosporylation-induced protein conformational changes in solution is based on (i) a decrease in the protein stability and (ii) an increase in the diameter of the protein particle, as seen by gel filtration chromatography and DLS. They indicate that the activation mechanism affects protein stability and dynamics in solution, both at the levels of the core and full-length NP, suggesting that the activated protein could adopt a more fluctuating conformation. Crystal-packing, i.e., the rigidity imposed by crystal contacts, might hamper the phosphorylation-induced protein expansion that is readily observed in solution and explains the strong destabilization of the protein particle. On the other hand, this "swelling" probably affects mainly flexible regions of the protein, less defined in the crystal structure (see below); therefore, it is not reflected in the crystal structure of the active mutant. This apparent contradiction underscores the usefulness of combining crystallography with solution techniques, as well as accounting for protein dynamics to explain functional aspects of protein activation.

Phosphorylation-mimicking mutation-induced destabilization of the protein, reflected in a steady decrease of ΔH_{cal}, T_m, and D_{50}, parallels the effect of phosphorylation on natural NP variants (*10, 15*). Both the destabilization and the expansion of the protein are probably due to electrostatic repulsion. The NP core domain folds into a remarkably stable and well-packed structure (*6*). However, the flexible N-terminal segment (residues 1−15), which bears some of the experimentally detected phosphorylation sites (*13*), is not resolved in the structure, and the loops between β strands 2 and 3 and between β strands 4 and 5 are also relatively mobile (*6*). The loops and at least the last residues of the N-terminal segment are oriented toward the distal face of the pentamer and are characterized by higher *B* factors in the crystal structure, which is related to their flexibility. Phosphorylation of residues in those areas would cause electrostatic repulsion and consequently an expansion of the flexible regions in the pentameric particle with a minor impact on the secondary structure of the monomer. The tertiary/quaternary structural levels would be secured by the hyperstable hydrophobic subunit interface, that serves as a stable scaffold allowing activation. This role of the structured core domain is essential when the full-length protein is considered.

As has been recently demonstrated, full protein activation requires phosphorylation of both protein domains (*13*). The tail domain of NP, in contrast to the core domain, folds into a natively disordered conformation, as is predicted (*11*) and has been suggested on the basis of IR and CD studies of deletion mutants (*9*). Phosphorylation or mutation-induced activation of the full-length protein adds more negative charges to each subunit of the pentamer and therefore increases the Columbic repulsive force that further destabilizes the protein. Mutations in the tail domain induce a greater expansion of the protein, as evidenced by a diameter increase of 4−4.4 and 1.4−3 Å for NP5D and NP8D, respectively, as compared with the wild-type protein. Note that although the number of added charges in NP8D is higher than in NP5D, the latter experiences the larger expansion. Therefore, while mutations in the core (in fixed positions) are more destabilizing, those in the tail (or in general, in flexible regions) have a more expanding effect, and probably this is the reason why they are better tolerated in terms of stability. In the case of the tail domain, it has been suggested that the oppositely charged polyglu tract and the NLS containing region might interact with each other in the full-length protein (*9*) and that phosphorylation of NLS flanking residues could modulate this interaction (*13*). If this were the case, phosphorylation of these residues, mimicked by mutations in NP5D, NP10D, and NP13D, would weaken the interaction, so that these disordered and flexible domains could be projected farther apart from the protein 5-fold axis. This situation most likely applies to hyperphosphorylated natural egg NP, that shows a diameter increase of 10 and 6 Å, as compared to recombinant wtNP and oocyte NP, respectively (*39*). Charging and activating the core domain results in an expansion of the full-length protein (NP8D) smaller than that of the isolated core domain (CORE8D), which may indicate that the previously suggested (*15*) interaction between the tail and the core domains could regulate the final swelling upon activation.

Protein phosphorylation is one of the posttranslational modifications most widely used to regulate protein activity (*37, 38*). The functional consequence of phosphorylation comes from structural effects of the phosphoryl groups attached to the protein that, depending on the protein under study, can promote stabilization or

destabilization (*40*−*44*). Both the phosphorylation-induced stabilization and destabilization can be local (*40, 41*), or global (*42*−*44*), as is the case for NP. The remarkable stability of the core domain will help the protein to cope with the strong electrostatic destabilization associated with its activation. However, it is also true that phosphorylation of particular residues of NP might modulate specific protein functions, as reported for the apoptosis-associated phosphorylation of Y127 (*45*). Massive phosphorylation of the pentameric protein, i.e., that found in natural egg NP, induces an expansion of the oligomer, which in turn could create a better binding surface involving flexible regions, particularly enriched in negatively charged residues, that could interact with oppositely charged ligands such as histones. Moreover, the phosphorylation-induced increase in negative potential could also modulate the binding affinity of the binding sites so that NP could efficiently compete with DNA for histone binding. One should note that upon binding histones or other basic proteins, (partial) neutralization of NP negative charge will reverse the activation-induced destabilization. In summary, our results show that accumulation of negative charge on NP, necessary to achieve activation, induces a destabilization of the protein. This effect is most probably due to electrostatic repulsion that weakens the quaternary interactions in the pentamer which are essential for the stability of this protein (*6, 15*). However, the loss of stability does not compromise, under physiological conditions, NP function or folding, which is granted by the extremely stable core domain. In fact, one could speculate that the reason for the extreme thermal stability of this protein from a mesophilic organism (*X. laevis*) is that it needs to afford a strong destabilization upon activation.

REFERENCES

1. Frehlick, L. J., Eirín-López, J. M., and Ausió, J. (2007) New insights into the nucleophosmin/nucleoplasmin family of nuclear chaperones. *BioEssays 29*, 49–59.
2. Prado, A., Ramos, I., Frehlick, L. J., Muga, A., and Ausió, J. (2004) Nucleoplasmin: a nuclear chaperone. *Biochem. Cell Biol. 82*, 437–445.
3. Akey, C. W., and Luger, K. (2003) Histone chaperones and nucleosome assembly. *Curr. Opin. Struct. Biol. 13*, 6–14.
4. Gillespie, P. J., and Blow, J. J. (2000) Nucleoplasmin-mediated chromatin remodelling is required for *Xenopus* sperm nuclei to become licensed for DNA replication. *Nucleic Acids Res. 28*, 472–480.
5. Tamada, H., Thuan, N. V., Reed, P., Nelson, D., Katoku-Kikyo, N., Wudel, J., Wakayama, T., and Kikyo, M. (2006) Chromatin decondensation and nuclear reprogramming by nucleoplasmin. *Mol. Cell. Biol. 26*, 1259–1271.
6. Dutta, S., Akey, I. V., Dingwall, C., Hartman, K. L., Laue, T., Nolte, R. T., Head, J. F., and Akey, C. W. (2001) The crystal structure of nucleoplasmin-core: implications for histone binding and nucleosome assembly. *Mol. Cell 8*, 841–853.
7. Namboodiri, H. V. M., Dutta, S., Akey, I. V., Head, J. F., and Akey, C. W. (2003) The crystal structure of *Drosophila* NLP-core provides insight into pentamer formation and histone binding. *Structure 11*, 175–186.
8. Namboodiri, H. V. M., Akey, I. V., Schmidt-Zachmann, M. S., Head, J. F., and Akey, C. W. (2004) The structure and function of *Xenopus* NO38-core, a histone chaperone in the nucleolus. *Structure 12*, 2149–2160.
9. Hierro, A., Arizmendi, J. M., Bañuelos, S., Prado, A., and Muga, A. (2002) Electrostatic interactions at the C-terminal domain of nucleoplasmin modulate its chromatin decondensation activity. *Biochemistry 41*, 6408–6413.
10. Hierro, A., Arizmendi, J. M., De las Rivas, J., Urbaneja, M. A., Prado, A., and Muga, A. (2001) Structural and functional properties of *Escherichia coli*-derived nucleoplasmin. A comparative study of recombinant and natural proteins. *Eur. J. Biochem. 268*, 1739–1748.
11. Sickmeier, M., Hamilton, J. A., Le Gall, T., Vacic, V., Cortese, M. S., Tantos, A., Szabo, B., Tompa, P., Chen, J., Uversky, V. N., Obradovic, Z., and Dunker, A. K. (2007) DisProt: the database of disordered proteins. *Nucleic Acids Res. 35*, D787−D793.
12. Cotten, M., Sealy, L., and Chalkley, R. (1986) Massive phosphorylation distinguishes *Xenopus laevis* nucleoplasmin isolated from oocytes or unfertilized eggs. *Biochemistry 25*, 5063–5069.
13. Bañuelos, S., Omaetxebarria, M. J., Ramos, I., Larsen, M. R., Arregi, I., Jensen, O. M., Arizmendi, J. M., Prado, A., and Muga, A. (2007) Phosphorylation of both nucleoplasmin domains is required for activation of its chromatin decondensation activity. *J. Biol. Chem. 282*, 21213–21221.
14. Bañuelos, S., Hierro, A., Arizmendi, J. M., Montoya, G., Prado, A., and Muga, A. (2003) Activation mechanism of the nuclear chaperone nucleoplasmin: role of the core domain. *J. Mol. Biol. 334*, 585–593.
15. Franco, G., Bañuelos, S., Falces, J., Muga, A., and Urbaneja, M. A. (2008) Thermodynamic characterization of nucleoplasmin unfolding: interplay between function and stability. *Biochemistry 47*, 7954–7962.
16. Ben-Bassat, A., Bauer, K., Chang, S. Y., Myambo, K., Boosman, A., and Chang, S. (1987) Processing of the initiation methionine from proteins: properties of the *Escherichia coli* methionine aminopeptidase and its gene structure. *J. Bacteriol. 169*, 751–757.
17. Kleywegt, G. J., and Brünger, A. T. (1996) Checking your imagination: applications of the free R value. *Structure 4*, 897–904.
18. Kissinger, C. R., Gehlhaar, D. K., and Fogel, D. B. (1999) Rapid automated molecular replacement by evolutionary search. *Acta Crystallogr., Sect. D: Biol. Crystallogr. 55*, 484–491.
19. Thompson, J. D., Higgins, D. G., and Gibson, T. J. (1994) CLUSTAL W: improving the sensitivity of progressive multiple sequence alignment through sequence weighting, position-specific gap penalties and weight matrix choice. *Nucleic Acids Res. 22*, 4673–4680.
20. Murshudov, G. N., Vagin, A. A., and Dodson, E. J. (1997) Refinement of macromolecular structures by the maximum-likelihood method. *Acta Crystallogr., Sect. D: Biol. Crystallogr. 53*, 240–255.
21. Jones, T. A., Zou, J.-Y., Cowan, S. W., and Kjeldgaard, M. (1991) Improved methods for building protein models in electron density maps and the location of errors in these models. *Acta Crystallogr. A47*, 110–119.
22. Cowtan, K., and Main, P. (1998) Miscellaneous algorithms for density modification. *Acta Crystallogr., Sect. D: Biol. Crystallogr. 54*, 487–493.
23. Laskowski, R. A., Moss, D. S., and Thornton, J. M. (1993) Main-chain bond lengths and bond angles in protein structures. *J. Mol. Biol. 231*, 1049–1067.
24. Kholodenko, V., and Freire, E. (1999) A simple method to measure the absolute heat capacity of proteins. *Anal. Biochem. 270*, 336–338.
25. Arnan, C., Saperas, N., Prieto, C., Chiva, M., and Ausió, J. (2003) Interaction of nucleoplasmin with core histones. *J. Biol. Chem. 278*, 31319–31324.
26. Sánchez-Ruiz, J. M., López-Lacomba, J. L., Cortijo, M., and Mateo, P. L. (1988) Differential scanning calorimetry of the irreversible thermal denaturation of thermolysin. *Biochemistry 27*, 1648–1672.
27. Kurganov, B. I., Lyubarev, A. E., Sánchez-Ruiz, J. M., and Shnyrov, V. L. (1997) Analysis of differential scanning calorimetry data for proteins. Criteria of validity of one-step mechanism of irreversible protein denaturation. *Biophys. Chem. 69*, 125–135.
28. Whitmore, L., and Wallace, B. A. (2008) Protein secondary structure analyses from circular dichroism spectroscopy: methods and reference databases. *Biopolymers 89*, 392–400.
29. Lees, J. G., Miles, A. J., Wien, F., and Wallace, B. A. (2006) A reference database for circular dichroism spectroscopy covering fold and secondary structure space. *Bioinformatics 22*, 1955–1962.
30. Salvany, L., Chiva, L., Arnan, C., Ausió, J., Subirana, J. A., and Saperas, N. (2004) Mutation of the small acidic tract A1 drastically reduces nucleoplasmin activity. *FEBS Lett. 576*, 353–357.
31. Freire, E., Murphy, K. P., Sánchez-Ruiz, J. M., Galisteo, M. L., and Privalov, P. L. (1992) The molecular basis of cooperativity in protein folding. Thermodynamic dissection of interdomain interactions in phosphoglycerate kinase. *Biochemistry 31*, 250–256.

32. Sánchez-Ruiz, J. M. (1995) Differential scanning calorimetry of proteins. *Subcell. Biochem. 24*, 133–176.
33. Georgescu, R. E., García-Mira, M. M., Tasayco, M. L., and Sánchez-Ruiz, J. M. (2001) Heat capacity analysis of oxidized *Escherichia coli* thioredoxin fragments (1−73, 74−108) and their noncovalent complex. Evidence for the burial of apolar surface in protein unfolded states. *Eur. J. Biochem. 268*, 1477–1485.
34. Pina, D. G., Gómez, J., Villar, E., Johannes, L., and Shnyrov, V. L. (2003) Thermodynamic analysis of the structural stability of the shiga toxin B-subunit. *Biochemistry 42*, 9498–9506.
35. Tholey, A., Lindermann, A., Kinzel, V., and Reed, J. (1999) Direct effects of phosphorylation on the preferred backbone conformation of peptides: a nuclear magnetic resonance study. *Biophys. J. 76*, 76–87.
36. Ramos, I., Prado, A., Finn, R. M., Muga, A., and Ausió, J. (2005) Nucleoplasmin-mediated unfolding of chromatin involves the displacement of linker-associated chromatin proteins. *Biochemistry 44*, 8274–8281.
37. Johnson, L. N., and Lewis, R. J. (2001) Structural basis for control by phosphorylation. *Chem. Rev. 101*, 2209–2242.
38. Graves, J. D., and Krebs, E. G. (1999) Protein phosphorylation and signal transduction. *Pharmacol. Ther. 82*, 111–121.
39. Hierro, A. (2002) Efecto de la fosforilación sobre la estructura y función de la nucleoplasmina, Ph.D. Thesis, University of the Basque Country.
40. Miranda, F. F., Teigen, K., Thórólfsson, M., Svebak, R. M., Knappskog, P. M., Flatmark, T., and Martínez, A. (2002) Phosphorylation and mutations of Ser(16) in human phenylalanine hydroxylase. Kinetic and structural effects. *J. Biol. Chem. 277*, 40937–40943.
41. Honnappa, S., Jahnke, W., Seelig, J., and Steinmetz, M. O. (2006) Control of intrinsically disordered stathmin by multisite phosphorylation. *J. Biol. Chem. 281*, 16078–16083.
42. Blanes-Mira, C., Ibáñez, C., Fernández-Ballester, G., Planells-Cases, R., Pérez-Payá, E., and Ferrer-Montiel, A. (2001) Thermal stabilization of the catalytic domain of botulinum neurotoxin E by phosphorylation of a single tyrosine residue. *Biochemistry 40*, 2234–2242.
43. Nosworthy, N. J., Peterkofsky, A., König, S., Seok, Y. J., Szczepanowski, R. H., and Ginsburg, A. (1998) Phosphorylation destabilizes the amino-terminal domain of enzyme I of the *Escherichia coli* phosphoenolpyruvate:sugar phosphotransferase system. *Biochemistry 37*, 6718–6726.
44. Ahmad, M. F., Raman, B., Ramakrishna, T., and Rao, Ch. M. (2008) Effect of phosphorylation on alpha B-crystallin: differences in stability, subunit exchange and chaperone activity of homo and mixed oligomers of alpha B-crystallin and its phosphorylation-mimicking mutant. *J. Mol. Biol. 375*, 1040–1051.
45. Lu, Z., Zhang, C., and Zhai, Z. (2005) Nucleoplasmin regulates chromatin condensation during apoptosis. *Proc. Natl. Acad. Sci. U.S.A. 102*, 2778–2783.

BI800975R